

# Exceptional power density and stability at intermediate temperatures in protonic ceramic fuel cells

Sihyuk Choi¹, Chris J. Kucharczyk¹,², Yangang Liang³, Xiaohang Zhang³, Ichiro Takeuchi³, Ho-II Ji <sup>□</sup>¹,² and Sossina M. Haile¹\*

Over the past several years, important strides have been made in demonstrating protonic ceramic fuel cells (PCFCs). Such fuel cells offer the potential of environmentally sustainable and cost-effective electric power generation. However, their power outputs have lagged behind predictions based on their high electrolyte conductivities. Here we overcome PCFC performance and stability challenges by employing a high-activity cathode,  $PrBa_{0.5}Sr_{0.5}Co_{1.5}Fe_{0.5}O_{5+\delta}$  (PBSCF), in combination with a chemically stable electrolyte,  $BaZr_{0.4}Ce_{0.4}Y_{0.1}Yb_{0.1}O_3$  (BZCYYb4411). We deposit a thin dense interlayer film of the cathode material onto the electrolyte surface to mitigate contact resistance, an approach which is made possible by the proton permeability of PBSCF. The peak power densities of the resulting fuel cells exceed 500 mW cm<sup>-2</sup> at 500 °C, while also offering exceptional, long-term stability under CO<sub>2</sub>.

rotonic ceramic fuel cells (PCFCs) incorporate a proton-conducting oxide as the electrolyte material. Like other fuel cells, they enable direct electrochemical conversion of chemical fuels to electricity at high efficiency and with zero emissions. They are particularly attractive in comparison to other fuel cells as a consequence of the high ionic conductivity of the electrolyte at at intermediate temperatures (400–600°C)¹. It is widely recognized that high-power operation in this temperature regime is key to lowering fuel cell costs. However, only a handful of studies report peak power densities of PCFCs exceeding 200 mW cm<sup>-2</sup> at 500°C²-5, whereas such performance is routine for traditional solid oxide fuel cells based on lower conductivity oxide-ion conducting electrolytes<sup>6-9</sup>. A further challenge in PCFC development lies in the reactivity of many protonic ceramic electrolytes with CO<sub>2</sub>, precluding their use at intermediate temperatures with carbon containing fuels¹.

The poor rate of oxygen electroreduction at the cathode of PCFCs has been recognized as one of the key factors limiting power densities in such fuel cells<sup>1</sup>. The reaction is written globally as

$$\frac{1}{2}O_2(gas) + 2e^-(cathode) + 2H^+(electrolyte) \rightarrow H_2O (gas)$$
 (1)

where it is implied, from the formalism of the expression, that the cathode, which also serves as the electrocatalyst, is electronically conductive but ionically insulating, and that the reaction is limited to the triple-phase boundary lines at which cathode, electrolyte and gas are in mutual contact. Experience with traditional SOFCs indicates that the best cathode electrocatalysts are those with mixed ionic and electronic conductivity. Such mixed conductivity opens up the reaction sites beyond the triple phase boundaries, to include the entire surface of the cathode material. While mixed oxide ion and electron conductors (MIECs) are well known and have been routinely employed in SOFC cathodes, deliberate creation of analogous proton and electron conductors has met with limited success <sup>10-12</sup>.

The majority of PCFC demonstrations have instead utilized the same types of materials used in traditional SOFCs (Supplementary Table 1). The efficacy of these cathode materials for oxygen electroreduction in PCFCs has led some authors to conclude that some conventional MIECs can, in fact, absorb H<sub>2</sub>O and thereby become good proton conductors (in addition to conducting oxide ions and electrons)<sup>13–15</sup>. Such materials have been termed 'triple conducting oxides' and the evident proton uptake justifies an examination of conventional MIECs for further PCFC development.

Beyond high polarization losses at the cathode, review of the PCFC literature, in which the vast majority of efforts rely on an electrolyte of composition  $BaZr_{0.1}Ce_{0.7}Y_{0.2-x}Yb_xO_3$  (x = 0 or 0.1), reveals a surprisingly high ohmic resistance in cells operated at moderate temperatures. For example, Nien et al.4, who achieved a notable peak power density of 587 mW cm<sup>-2</sup> at 500 °C (with dry O<sub>2</sub> as the oxidant rather than standard air), reported an ohmic area-specific resistance (ASR) of  $0.45 \Omega$  cm<sup>2</sup>. For the  $18 \mu m$  thick electrolyte used in that work, the expected ASR is only  $\sim 0.12 \Omega$  cm<sup>2</sup>. Similarly, Nguyen et al.<sup>2</sup> reported an ohmic ASR of  $0.24\Omega$  cm<sup>2</sup> in their cell, which achieved a peak power density of 230 mW cm<sup>-2</sup> at 500 °C, although the electrolyte would be expected to have an ASR of only  $0.06 \Omega$  cm<sup>2</sup>. Even after eliminating otherwise resistive grain boundaries in their 2.5 µm thick electrolyte, which in this case was BaZr<sub>0.85</sub>Y<sub>0.15</sub>O<sub>3</sub> (BZY15), Bae et al.<sup>5</sup> found an ohmic ASR of  $0.15\,\Omega$  cm<sup>2</sup>. This resistance is low on an absolute scale and contributed to the impressive peak power density of 457 mW cm<sup>-2</sup>. However, the ohmic resistance was still more than eight times greater than expected. Such a discrepancy between expected and observed ohmic ASR appears also in several reports for cells of poorer performance, Supplementary Table 1.

In the present work we integrate three advances in PCFCs. First, we demonstrate exceptional proton solubility and transport through PBSCF, properties which render it ideal for oxygen electroreduction in PCFCs. Second, we establish that high ohmic losses have been a large part of the cause of poor cell performance to date

<sup>1</sup>Materials Science and Engineering, Northwestern University, Evanston, IL, USA. <sup>2</sup>Applied Physics & Materials Science, California Institute of Technology, Pasadena, CA, USA. <sup>3</sup>Materials Science and Engineering, University of Maryland, College Park, MD, USA. \*e-mail: sossina.haile@northwestern.edu

and design a strategy to address this challenge. While many factors can be manifest as ohmic losses, including decreases in electrolyte conductivity, due to effects such as limited grain growth, loss of barium during high temperature processing, or incorporation of Ni from the anode, the electrolyte selection and fabrication processes in the literature studies render these factors somewhat unlikely. We speculated that instead, poor contact between cathode and electrolyte was responsible for the high resistance values and overcome this obstacle using advanced processing methods. Third, to address stability and processability challenges with known electrolytes, we introduce a compositional variant in the barium zirconate – barium cerate class, combining high stability with excellent processability and outstanding conductivity.

# **Materials**

The electrolyte material of the present study, BZCYYb4411, combines the chemical stability and bulk proton conductivity afforded by doped barium zirconate with the ease of sintering and grain growth afforded by doped barium cerate, a strategy also pursued in the BaCe<sub>0.8-x</sub>Zr<sub>x</sub>Y<sub>0.2</sub>O<sub>3</sub> and related systems<sup>16,17</sup>. BZCYYb4411 adopts a cubic crystal structure, Supplementary Fig. 1, with lattice constant a = 4.3060(1) Å, and remains free of barium carbonate after prolonged exposure to 100 % carbon dioxide at 500 °C, Fig. 1a. No weight gain indicative of carbonate formation is evident by thermogravimetric analysis, Fig. 1b. A strong correlation between tolerance factor, tendency towards cubic symmetry, and thermodynamic stability (as measured in terms of the energy of formation from the component oxides) has been previously noted in the literature<sup>18–20</sup>,

and the behavior of BZCYYb4411 is consistent with these observations. The conductivity of polycrystalline BZCYYb4411 is approximately three times greater than that of BaZr<sub>0.8</sub>Y<sub>0.2</sub>O<sub>3</sub> (BZY20)<sup>21</sup>, Fig. 1c, for compacts of similar densities prepared under similar conditions, specifically, sintered at 1600 °C for 24 h under static air, with care taken to minimize effects of possible barium loss. This difference in transport properties is in large part due to the much greater grain growth in BZCYYb4411. The resulting grains are 4–5 μm in size, Fig. 1d, as compared to a mean grain size in BZY20 of  $\sim 0.44 \, \mu \text{m}$ , reflecting the highly refractory nature of the latter<sup>22</sup>. Additional benefit arises from the slightly higher bulk conductivity of BZCYYb4411, Supplementary Fig. 2, a surprising result given the prevalent view that BZY20 has the highest bulk conductivity amongst proton conducting oxide materials1. Compositions with the dopants Y and Yb replaced with single dopants 20 % Y, 20 % Yb and 20 % Ho displayed similar chemical stability, Supplementary Fig. 3, and the conductivities are only slightly lower than that of BZCYYb4411, Supplementary Fig. 2b. A lower cerium concentration of 20% maintains the stability, but the macroscopic conductivity falls slightly. In contrast, the composition BaZr<sub>0.1</sub>Ce<sub>0.7</sub>Y<sub>0.1</sub>Yb<sub>0.1</sub>O<sub>3</sub> (BZCYYb1711), which is known to have high conductivity and has been the electrolyte in several important PCFC studies<sup>2,3,17,23,24</sup>, was observed here to react with CO<sub>2</sub>, Supplementary Fig. 4.

The cathode, PBSCF, was selected on the basis of the high activity of the related material NdBa $_{0.5}$ Sr $_{0.5}$ Co $_{1.5}$ Fe $_{0.5}$ O $_{5+\delta}$  (NBSCF), from which PCFC cells with peak power density of 690 mW cm $^{-2}$  at 600 °C have been obtained $^{24}$ . This is amongst the highest values in the open literature at 600 °C, approaching results achieved using Sm $_{0.5}$ Sr $_{0.5}$ CoO $_{3.\delta}$ 

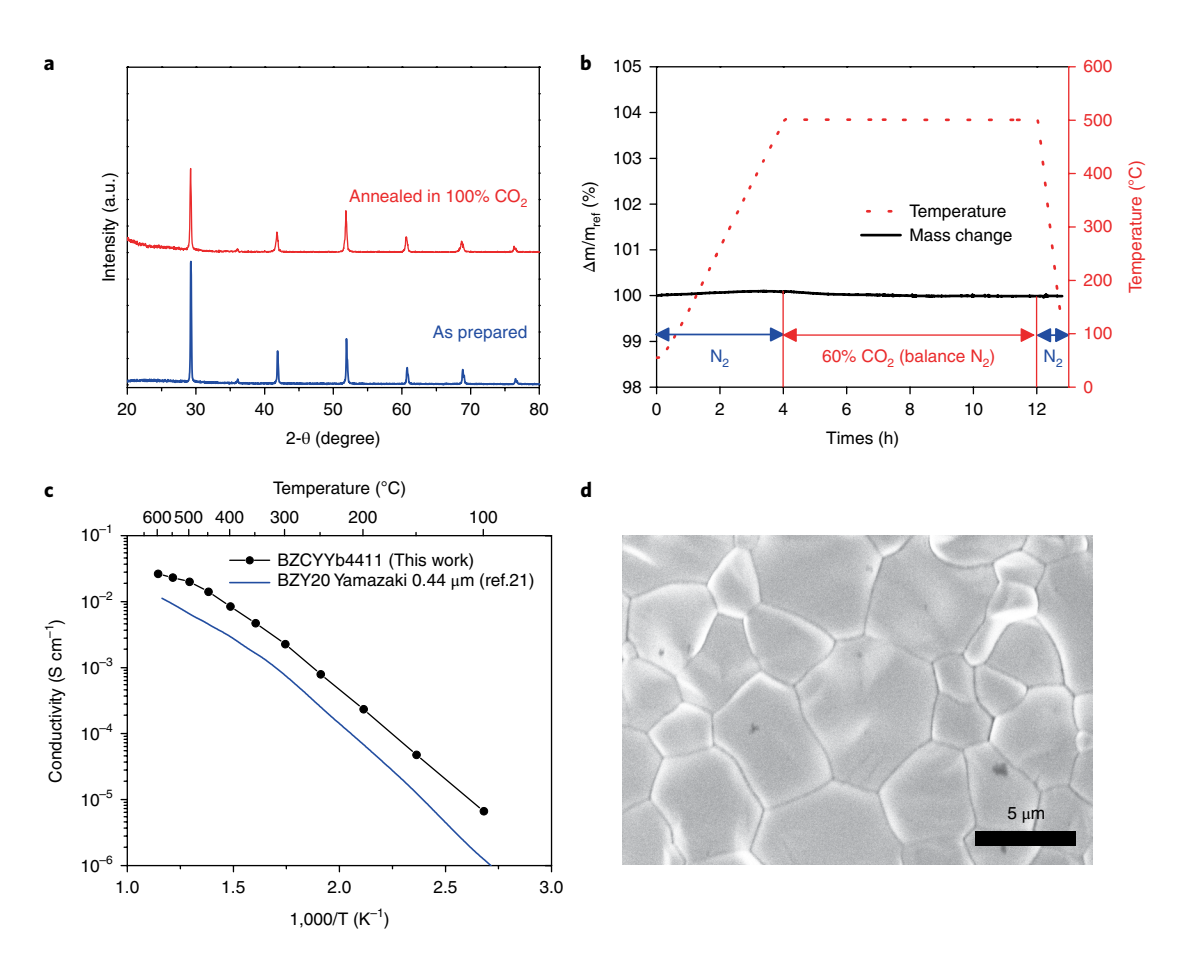


**Fig. 1** Selected characteristics of the electrolyte material BZCYYb4411. a, XRD pattern before and after exposure to 100 %  $CO_2$  at 500 °C. b, TGA profile on exposure to 60 %  $CO_2$  (balance  $N_2$ ) at 500 °C. c, Conductivity under humidified  $N_2$  atmosphere ( $pH_2O = 0.031$  atm) as compared to that of BZY20 sintered under similar conditions (ref. 21). d, SEM image of the as-sintered surface morphology.

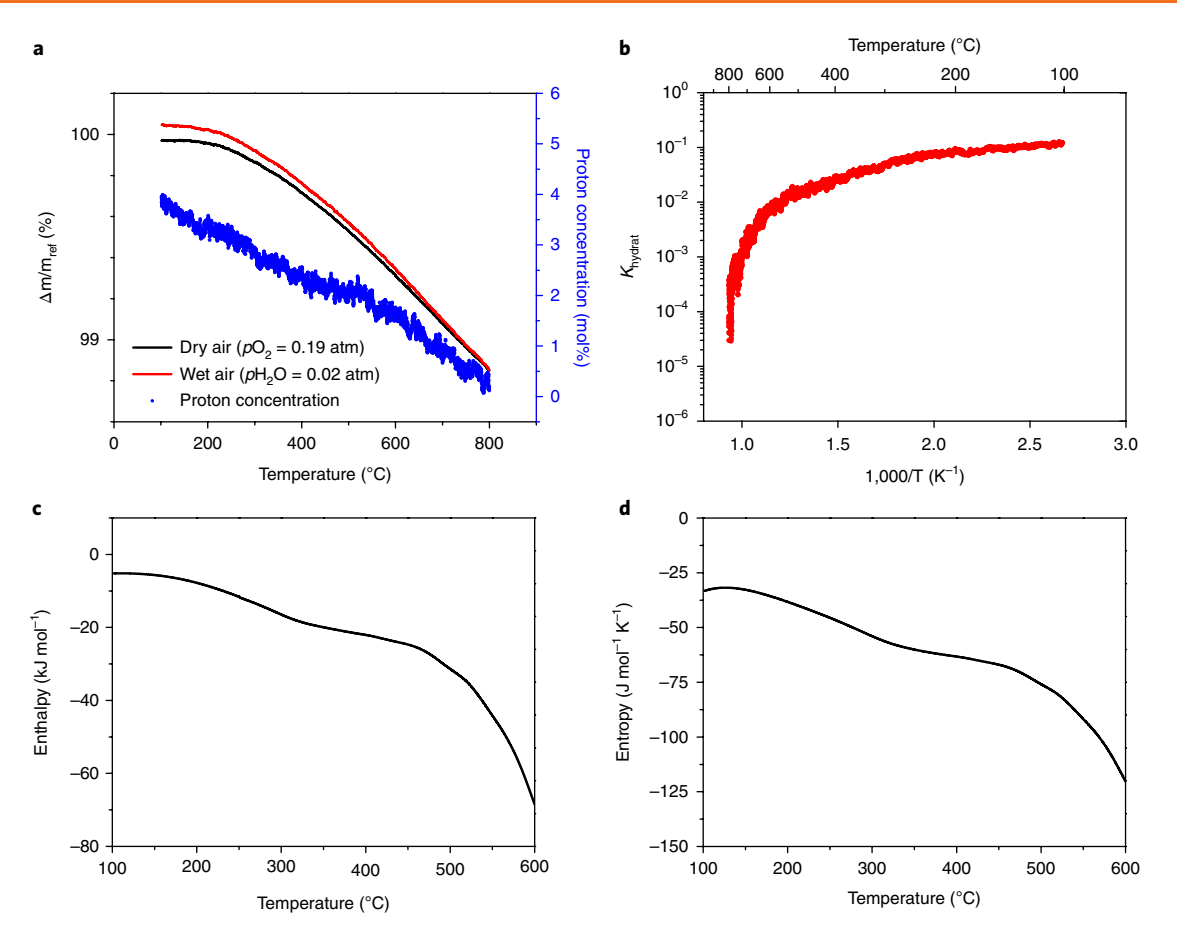


**Fig. 2** | **H**<sub>2</sub>**O** uptake behavior of PBSCF. **a**, Thermogravimetric profiles on cooling in dry and wet air and implied proton concentration. **b**, Equilibrium constant for the hydration reaction. **c**, Enthalpy of hydration. **d**, Entropy of hydration. Thermodynamic properties in (**c**) and (**d**) are obtained from analysis of the van't Hoff plot given in (**b**) after smoothing to remove spurious effects resulting from the subtraction of mass values given in (**a**).

(SSC)<sup>4</sup> and La<sub>0.6</sub>Sr<sub>0.4</sub>CoO<sub>3.8</sub> (LSC)<sup>5</sup> and exceeding those obtained using the designer mixed proton-electron (and oxide ion) conductor BaCo<sub>0.4</sub>Fe<sub>0.4</sub>Zr<sub>0.1</sub>Y<sub>0.1</sub>O<sub>3.8</sub> as cathodes. The Pr analog offers potential advantages as a result of its slightly higher electronic conductivity; its activity in conventional SOFCs is also slightly higher.<sup>9</sup>.

Both PBSCF and NBSCF are double-perovskites of general composition LnA'B<sub>2</sub>O<sub>5+ $\delta$ </sub> (Ln=La, Pr, Nd, Sm, Gd; A'=Ba, Sr; and B=Co, Fe, Mn), in which the A cation of the architype ABO<sub>3</sub> perovskite is replaced in alternating fashion with Ln and A' cations. The result is a layered structure with stacking sequence ...  $[A'O]-[BO_2]-[LnO_\delta]-[BO_2]...$  along the c-axis<sup>25,26</sup>. Kim et al. showed that the bulk oxygen diffusivity and surface reaction constant of the representative double perovskite PrBaCo<sub>2</sub>O<sub>5+8</sub> are much higher than those of standard perovskite MIEC cathode materials<sup>26</sup>, spawning a surge in efforts to exploit these materials for conventional SOFCs<sup>6,9,25,27-31</sup>. The diffusivity is particularly high normal to [001], in the plane of high oxygen vacancy concentration<sup>32</sup>. Exploration of double-perovskites in PCFC systems is at a nascent stage (only three examples in Supplementary Table 1). Furthermore, at least in the case of PrBaCo<sub>2</sub>O<sub>5+8</sub>, the capacity for H<sub>2</sub>O uptake, a prerequisite for oxygen reduction in PCFC systems via a doublephase boundary pathway, is in some dispute<sup>14,15,33</sup>. These factors drive our evaluation of PBSCF from both performance and mechanistic perspectives.

# Compatibility and H<sub>2</sub>O uptake characteristics of PBSCF

We first checked for chemical compatibility between the electrolyte and PBSCF. Powders of the cathode and electrolyte materials were combined in a 1:1 weight ratio, milled, compacted together, then heat treated at 900, 1000 and 1100 °C for 24h under static air. The diffraction patterns obtained subsequent to these treatments are fully described by a superposition of the two individual components, Supplementary Fig. 5. We then evaluated the extent of  $\rm H_2O$  uptake into PBSCF by thermogravimetric analysis (TGA). The mass of the material (in loose powder form) was recorded as a function of temperature under humidified ( $p\rm H_2O=0.020\,atm$ ) and under dry synthetic air ( $p\rm O_2=0.19\,atm$ , balance  $\rm N_2$ ) between 800 and 100 °C. A clear difference in mass under the two atmospheres is evident at all temperatures below 800 °C, Fig. 2a and Supplementary Fig. 6. Attributing this difference to  $\rm H_2O$  uptake into the bulk implies a proton concentration that ranges from 3.5 mol % at 200 °C to 1.7 mol % at 600 °C.

These proton uptake results enable evaluation of the thermodynamics of the hydration reaction, Eq. (2), with associated equilibrium constant given in Eq. (3):

$$H_2O + V_O^{\bullet \bullet} + O_o^{\times} \leftrightarrow 2OH_O^{\bullet}$$
 (2)

$$K_{\mathrm{W}} = \frac{\left[\mathrm{OH}_{\mathrm{O}}^{\bullet}\right]^{2}}{p\mathrm{H}_{2}\mathrm{O}\left[\mathrm{V}_{\mathrm{O}}^{\bullet}\right]\left[\mathrm{O}_{\mathrm{O}}^{\times}\right]} = exp\left(\frac{\Delta_{\mathrm{W}}S}{R}\right) \exp\left(-\frac{\Delta_{\mathrm{W}}H}{RT}\right) \tag{3}$$

where  $[OH_O^{\bullet}]$ ,  $[V_O^{\bullet\bullet}]$ , and  $[O_O^{\times}]$  are, respectively, the proton (hydroxyl), oxygen vacancy, and oxygen concentrations in the

hydrated state;  $\Delta_W S$  and  $\Delta_W H$  are the entropy and enthalpy, respectively, of the hydration reaction; and R and T are, respectively, the universal gas constant and temperature. The TGA results under synthetic air, Supplementary Fig. 7, were used to determine the oxygen vacancy concentration under dry conditions using an oxygen stoichiometry of 5.88 at 100 °C as a reference<sup>30</sup>. The site concentrations under wet conditions, Supplementary Fig. 8, were then obtained according to

$$[O_O^{\times}]^{wet} = [O_O^{\times}]^{dry} - \frac{1}{2}[OH_O^{\bullet}]$$
 (4)

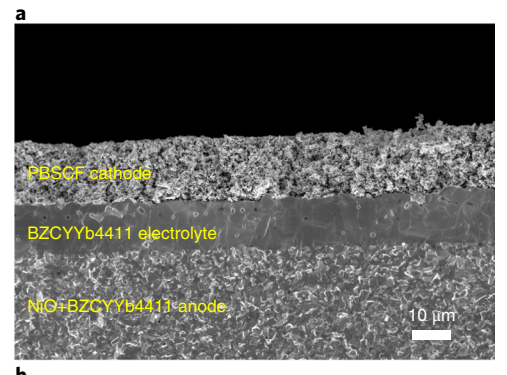
$$[V_O^{\bullet\bullet}]^{wet} = [V_O^{\bullet\bullet}]^{dry} - \frac{1}{2}[OH_O^{\bullet}]$$
 (5)

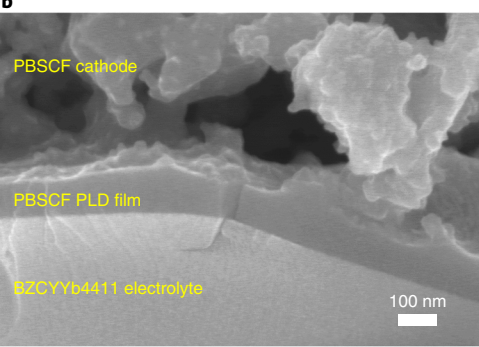
A negligible change in electronic defect concentration in response to reaction with steam is implicitly assumed.

From an evaluation of the temperature dependence of  $K_{w}$ , shown in the van't Hoff plot in Fig. 2b, we extract enthalpy and entropy values of -22 kJ mol<sup>-1</sup> and -63 J mol<sup>-1</sup> K<sup>-1</sup>, respectively, at 400 °C. In principle, a van't Hoff analysis should be performed at fixed stoichiometry (rather than fixed chemical potential) and the significant non-linearity in the present van't Hoff plot may be a result of the changing hydration state with temperature. In addition electronic defects can become important at high temperature<sup>34-36</sup> and contribute to non-linearity. Nevertheless, the thermodynamic values can be compared to those reported for other oxides considered for either electrolyte or cathode applications, for which analogous analysis methodologies are employed. In this context, both the enthalpy and entropy obtained here are small in magnitude, where typical values range from -20 to -170 kJ mol<sup>-1</sup> and -90 to -180 J mol<sup>-1</sup> K<sup>-1</sup>, respectively<sup>36</sup>. The entropy is particularly far from the range of observed values and is much smaller in magnitude than has been reported for  $Ba_{0.5}Sr_{0.5}Fe_{0.8}Zn_{0.2}O_{3-\delta}$  and  $BaCo_{0.4}Fe_{0.4}Zr_{0.2}O_{3-\delta}$ (respectively,  $-145\pm30$  and  $-103\pm5$  J mol<sup>-1</sup> K<sup>-1</sup>), the only other 'triple conducting oxide' for which the thermodynamics have been determined<sup>36,37</sup>. Thus, the entropic penalty of hydrating the doubleperovskite is small in comparison to other materials and correlates with the much higher proton content. For example, the proton concentration in BaCo<sub>0.4</sub>Fe<sub>0.4</sub>Zr<sub>0.2</sub>O<sub>3-δ</sub> is just 0.5 mol% (equivalent to 1.0 mol% for comparison to the double perovskite) at 400 °C in 0.065 atm pH<sub>2</sub>O<sup>37</sup>. Whether this is a universal difference between standard and double-perovskite materials, resulting from the different configurations available to dissolved hydroxyl groups, remains to be addressed. Significant also is the extremely rapid mass response to the imposed temperature steps, with mass increasing almost entirely in synchronization with the temperature during each cooling step of a stepwise experiment reported in Supplementary Fig. 6. Such fast mass changes imply rapid migration of all the relevant ionic defects of Eq. (2).

# Fuel cell design and electrochemical evaluation

We then prepared anode-supported cells incorporating neat PBSCF as the cathode and Ni + BZCYYb4411 as the anode. A mixture of NiO, BZCYYb4411, and starch (a fugitive pore-former) were combined in a weight ratio of 65:35:5, milled, then pressed into a disc and lightly sintered at 800 °C for 4h. A thin layer of BZCYYb4411 was subsequently applied by drop-casting. After removal of organics from the electrolyte layer at 400 °C, the anode-electrolyte bi-layer structure was sintered at 1500 °C for 4h. With the aim of addressing the apparently poor cathode-electrolyte contact in a typical SOFC fabrication, we applied the cathode layer by two different approaches. In one case, we followed a typical procedure in which a slurry of PBSCF was directly painted onto the electrolyte surface. In the second case, we first applied a thin (~100 nm) layer of PBSCF





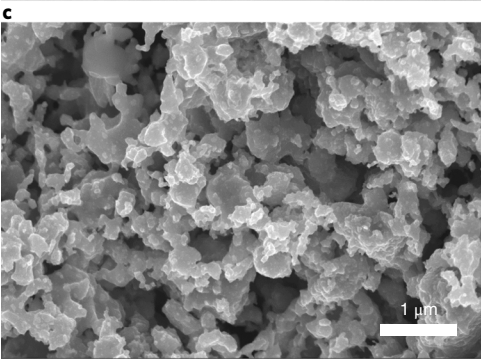


**Fig. 3 | Scanning electron microscopy images of PBSCF/BZCYYb4411/ cermet anode fuel cell. a**, Cross-section. **b**, Expanded view of cross-section showing PLD layer at the cathode of electrolyte-cathode interface. **c**, PBSCF cathode microstructure after sintering at 950 °C.

by pulsed laser deposition (PLD), on top of which the standard slurry was brush-painted. The final sintering step was carried out at 950 °C in air (4h). For both types of cells the electrolyte was  $\sim$  15  $\mu$ m thick and the cathode  $\sim$  20  $\mu$ m thick, Fig. 3a, with the PLD cathode layer forming a conformal coating onto the electrolyte, Fig. 3b, and the cathode retaining good porosity after the final sintering step, Fig. 3c. Ag wires were attached to both electrodes and electrical behaviour was measured in a pseudo-four probe configuration (eliminating the resistance of the lead wires).

The polarization behaviour, Fig. 4, collected with humidified  $\rm H_2$  supplied to the anode and synthetic air to the cathode, reveals exceptionally high activity for the PBSCF cathode. Even for the conventionally prepared cell, the peak power density at 600 °C exceeds 800 mW cm<sup>-2</sup>. Application of the PLD layer resulted in a marked increase in power output. The peak power density at 600 °C becomes 1098 mW cm<sup>-2</sup>, surpassing all previous records, including the 747 mW cm<sup>-2</sup> attained using SSC as the cathode and dry  $\rm O_2$  as the oxidant<sup>4</sup> (where the latter typically boosts the voltage relative to conventional operation on air). At 500 °C, the peak power density of 548 mW cm<sup>-2</sup> exceeds the value of 455 mW cm<sup>-2</sup> reported

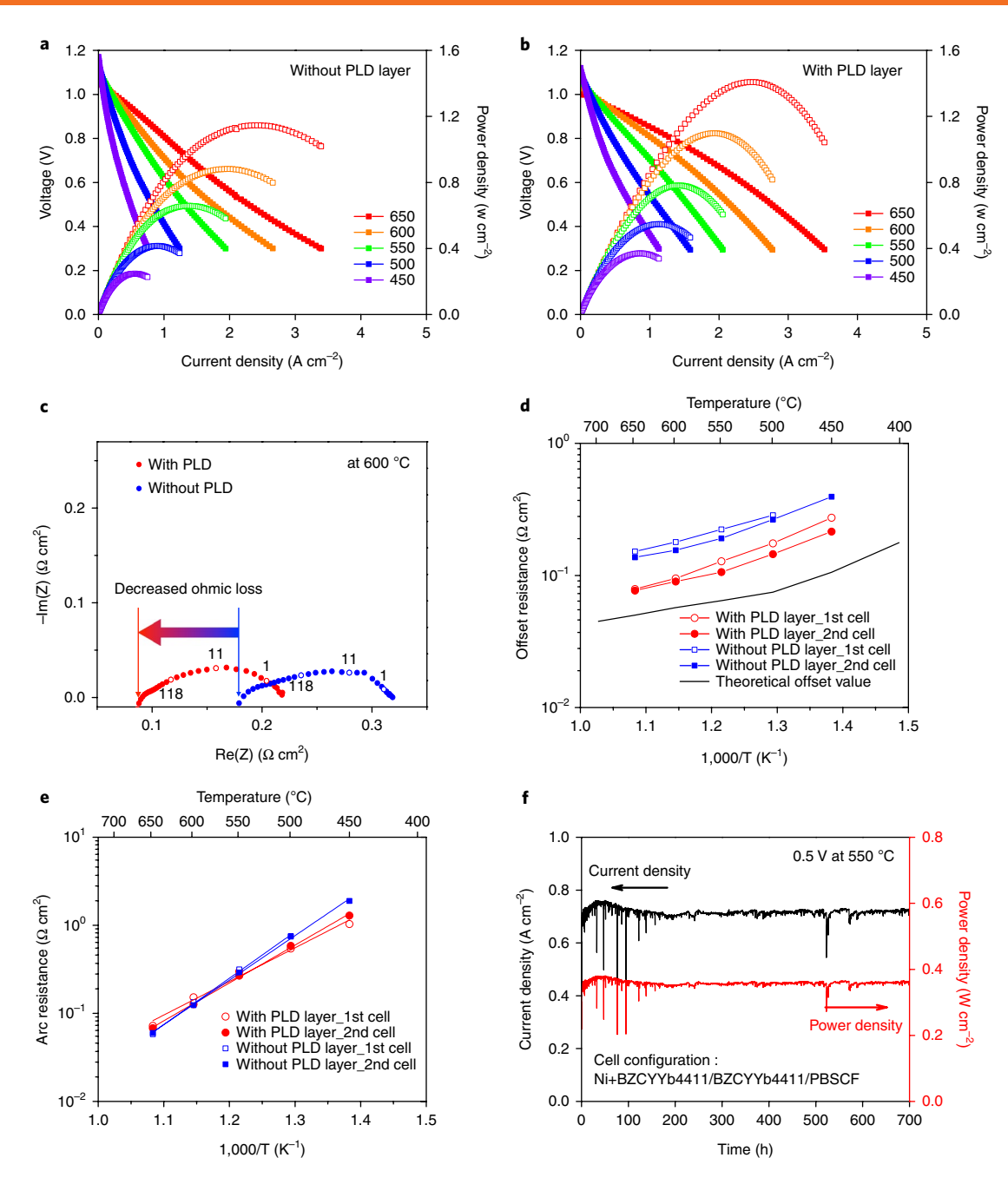
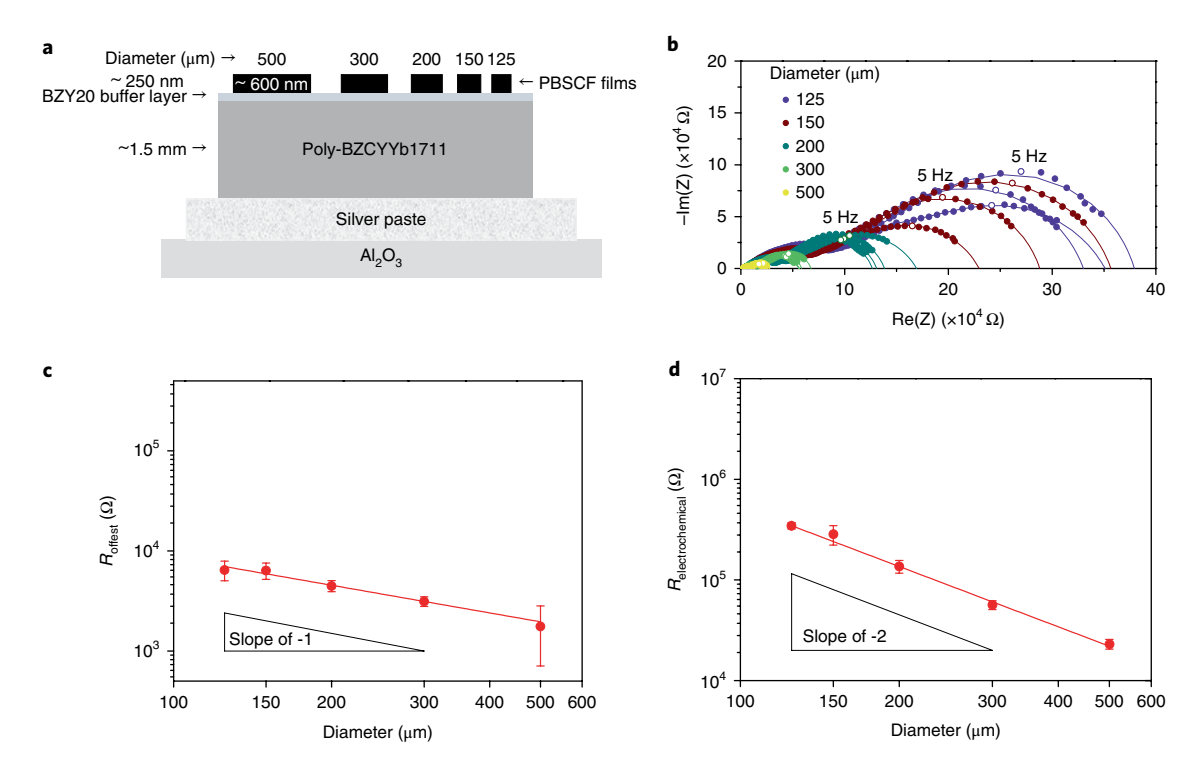


Fig. 4 | Electrochemical properties of the PBSCF cathode based on BZCYYb4411 proton conducting electrolyte using humidified (3%  $H_2O$ )  $H_2$  as fuel and dry air as oxidant at various temperatures. a, Polarization and power density curves of a representative cell without a PLD layer. b, Polarization and power density curves of a representative cell with a PLD layer. c, Impedance spectra collected at 600 °C, showing dramatic decrease in offset resistance on introduction of the cathode PLD layer. d, Offset (ohmic) resistance under OCV. e, Electrochemical reaction (arc) resistance under OCV. f, Temporal evolution of the cell current density and power density under a constant voltage load of 0.5 V at 550 °C in humidified  $H_2$ .

for  $BaCo_{0.4}Fe_{0.4}Zr_{0.1}Y_{0.1}O_{3.\delta}^3$ , a material explicitly designed to display protonic conductivity, in addition to electronic and oxygen ion conductivity. The significant contribution of the PBSCF as compared to other aspects of the cell design was configured by evaluating a similarly prepared cell in which  $La_{0.6}Sr_{0.4}Co_{0.2}Fe_{0.8}O_{3.\delta}$  (LSCF) served as the cathode, Supplementary Fig. 9. Using LSCF, peak power densities of only 519 and 201 mW cm<sup>-2</sup> were obtained at 600 and 500 °C, respectively. Overall, the behaviour reported here competes with that of high performance SOFCs based on oxide ion conductors. The possibility that Ag in the current collector contributes non-trivially to the measured activity was eliminated by the

observation of low power density from a cell in which the PBSCF was omitted and only Ag paste was utilized, Supplementary Fig. 10.

To elucidate the role of the cathode PLD layer, we measured the A.C. electrical impedance under open circuit conditions, enabling deconvolution of the various contributions to the overall cell resistance. Plotted in the complex plane, each impedance spectrum showed a single, depressed arc, attributed to the electrochemical reaction resistance, with a finite offset from the origin, representing the ohmic losses (Fig. 4c). Application of the PLD layer dramatically decreased the offset resistance in Fig. 4d, implying an improvement in the cathode-electrolyte contact as intended. In contrast, it



**Fig. 5 | Electrochemical behavior of microdot PBSCF at 500 °C under lightly humidified synthetic air as determined from a.c. impedance spectroscopy. a**, Schematic of sample configuration. **b**, Raw impedance spectra and the corresponding fit curves as function of electrode diameter. **c**, Offset resistance (largely due to electrolyte). **d**, electrochemical reaction resistance. Triangles indicate slopes of −1 and −2, respectively, in the double logarithmic plots. The errors bars correspond to standard deviations from the averaging across all measurements.

had only a slight impact on the electrochemical resistance, marginally decreasing the activation energy such that this resistance contribution was slightly decreased in the lower temperature regime, Fig. 4e. These characteristics were reproducibly observed in two pairs of cells, as indicated in Fig. 4d and e, and in additional cells evaluated only at high temperature (Supplementary Fig. 11). It is to be noted that even with the PLD layer, the cell offset resistance remains higher than that implied by the properties of the electrolyte. The source of the discrepancy is unknown.

We then examined the stability of our cell components by evaluating two cells (each prepared without a PLD layer) for prolonged periods. In one case we measured the open circuit voltage (OCV) upon exposure of the anode to a humidified mixture of CO<sub>2</sub> and H<sub>2</sub>, and in the second we measured the current upon exposure to humidified hydrogen at a constant cell voltage. Under both conditions, the cells display excellent stability. As measured over a 100 h period, the OCV deviates from the initial value by no more than 1 % (Supplementary Fig. 12a). In contrast, an analogous BZCYYb1711 based-cell shows an 86 % OCV loss after just 20 h of measurement (Supplementary Fig. 12b). At constant voltage, Fig. 4f, excellent stability is also observed, in this case after a break-in period of approximately 150 h. The morphological features of the cell appeared unchanged by the 700 h measurement, Supplementary Fig. 13.

# Oxygen electrochemical reduction pathway on PBSCF

The high performance and the high H<sub>2</sub>O uptake into PBSCF suggest that the oxygen electrochemical reaction occurs by a double-rather than triple-phase boundary pathway, with protons migrating through the bulk of the PBSCF and reacting with oxygen at the cathode/gas interface. Such a pathway is strongly indicated by the observation that a dense PBSCF layer on the cathode side of the electrolyte enhances rather than diminishes cell performance. Indeed, while application of similar PLD-derived dense films to

improve contact between electrolyte and cathode in conventional SOFCs has been suggested<sup>38</sup>, success relies on the ion permeability of the cathode material. We directly examined the possibility of reaction via a double-phase boundary pathway by measuring the electrochemical properties of PBSCF thin film (~600 nm) microdot electrodes, deposited onto the surface of dense, polycrystalline BZCYYb1711 ~ 1.5 mm in thickness, Fig. 5a. To provide a smooth surface for electrode deposition, a thin (~250 nm) buffer layer of BZY20 was first applied. X-ray diffraction analysis confirmed the absence of reactivity between these components, and atomic force microscopy revealed the PBSCF surface to have a rms roughness of 43.8 nm, reflecting the roughness of the underlying polycrystalline substrate, Supplementary Fig. 14. We patterned the PBSCF film by ion milling to create sharply-defined microelectrodes ranging in diameter from 125 to 500 µm, with over ten duplicates of each diameter, Supplementary Fig. 15. We then measured the A.C. electrical impedance at each microelectrode, using an automated probe station described previously<sup>39</sup>. Data were recorded under 0.2 atm O<sub>2</sub> (balance Ar) at 500 °C after a 24 h stabilization period. Under these conditions, BZCYYb1711, like BZCYYb4411, is predominantly a proton conductor, ensuring that the electrochemical response measured here is that associated with reaction (1) as catalysed by PBSCF.

All impedance spectra could be adequately described by an equivalent circuit composed of a resistor ( $R_{\rm offset}$ ) in series with two subcircuits, each composed of a resistor in parallel with a constant phase element, Fig. 5b. Identification of the mechanistic origins of these two features is beyond the scope of the present work. For this initial study, the sum of these two resistances is taken to be the electrochemical reaction resistance ( $R_{\rm electrochemical}$ ). For the geometry considered (a semi-infinite conductor), the offset resistance is expected to be dominated by the resistance of the underlying electrolyte, with a scaling with diameter according to the Newman equation  $R_{\rm offset} = 1/(2\sigma D)$ , where  $\sigma$  and D are the electrolyte

conductivity and the microelectrode diameter, respectively. In accord with this expression, a double-logarithmic plot of  $R_{\rm offset}$  vs D, yields a line with a slope close to -1, Fig. 5c, and an implied conductivity of  $5.6\times10^{-3}\,\rm S~cm^{-1}$  at  $500\,^{\circ}\rm C$  (in reasonable agreement with the properties of BZCYYb1711). The electrochemical resistance is expected to be dominated by the properties of the microelectrode. Here, the double-logarithmic plot yields a slope of -2, which would result from a process occurring via a double-phase boundary pathway, Fig. 5d. That is, the data reveal that resistance scales inversely with area, implying that the entire surface of the microelectrode is electrochemically active. This feature, enabled in part by the high solubility of  $\rm H_2O$  into the oxide, undoubtedly contributes to the very activity of PBSCF for the oxygen reduction reaction in PCFCs.

## **Conclusions**

In sum, we demonstrate that fuel cells comprising the double-perovskite cathode PBSCF and the electrolyte BZCYYb4411 deliver both exceptional power densities and excellent long term stability in the highly prized intermediate temperature regime. The cathode has a high solubility for protons, a factor supporting electrochemical activity at the solid-gas interface, whereas the electrolyte provides a balance between the processability afforded by high cerium content and the high chemical stability afforded by high zirconium content. A dense layer of PBSCF, prepared by pulsed laser deposition, improves the contact between electrolyte and cathode, dramatically reducing ohmic losses as compared to cells without the PLD layer. While residual ohmic losses of unidentified origin remain, these advances pave the way for incorporating fuel cells into a sustainable energy future.

#### Methods

**Cathode preparation.** Powders of PrBa<sub>0.5</sub>Sr<sub>0.5</sub>Co<sub>1.5</sub>Fe<sub>0.5</sub>O<sub>5+6</sub> (PBSCF) were synthesized *via* a variant of the Pechini process in which nitrate precursors are dissolved in aqueous solution, and citric acid and ethylene glycol are used as complexing agents<sup>41</sup>. The char resulting from the gelation and drying steps was calcined at 600 °C to eliminate organic residue. The calcined powders were ball milled, then sintered at 1150 °C for 12 h to achieve single phase products as confirmed by X-ray diffraction (XRD) (Scintag XDS2000, Cu Kα radiation, 40 kV, 20 mA).

**Proton uptake measurement.** To evaluate proton uptake in PBSCF, TGA was carried out using a Netzsch STA 449 C on powder samples in dry and wet air. 200 sccm of synthetic air and 20 sccm Ar were supplied to the measurement chamber to obtain an oxygen partial pressure  $(pO_2)$  of 0.19 atm. For the wet air condition, the gas mixture was bubbled through a distilled water bubbler held at 18 °C to obtain a water partial pressure  $(pH_2O)$  of 0.020. Under both conditions, the sample temperature was first increased from 100 to 800 °C at 5 °C min<sup>-1</sup> and weight data then recorded upon cooling to 100 °C. Two sets of data were collected. In one case the temperature was continuously cooled at a rate of 0.5 °C min<sup>-1</sup> (Fig. 2a); in the second case the temperature decreased in 100 °C steps with a 3 h dwell at each step. Good agreement was obtained, particularly at 400 °C and higher (Supplementary Fig. 6), indicating equilibration of the sample at those temperatures.

Electrolyte preparation and characterization. The multi-component electrolyte oxides (Ba $Zr_{0.4}Ce_{0.4}Y_{0.2}O_3$  (BZCY442), Ba $Zr_{0.4}Ce_{0.4}Yb_{0.2}O_3$  (BZCYb442),  $BaZr_{0.4}Ce_{0.4}Ho_{0.2}O_{3} \ (BZCHo442), \ BaZr_{0.4}Ce_{0.4}Y_{0.1}Yb_{0.1}O_{3} \ (BZCYYb4411), \ BaZr_{0.4}Ce_{0.4}Yb_{0.1}O_{3} \ (BZCYYb44111), \ BaZr_{0.4}Ce_{0.4}Yb_{0.1}O_{3} \ (BZCYYb44111), \ BaZr_{0.4}Ce_{0.4}Yb_{0.1}O_{3} \ (BZCYYb44111), \ BaZr_{0.4}Ce_{0.4}Yb_{0.1}O_{3} \ (BZCYYb4111), \ BaZr_{0.4}Ce_{0.4}Yb_{0.1}O_{3} \ (BZCYYb4111), \ BaZr_{0.4}Ce_{0.4}$ Y<sub>0.1</sub>Yb<sub>0.1</sub>O<sub>3</sub> (BZCYYb1711)) were prepared by solid state reaction of stoichiometric quantities of barium carbonate (>99%, Sigma Aldrich), zirconium oxide (99.5%, Alfa Aesar), cerium oxide (99.9%, Alfa Aesar) and the oxides of the dopants, yttrium oxide (99.9%, Alfa Aesar), ytterbium oxide (99.9%, Alfa Aesar) and holmium oxide (99.9%, Alfa Aesar). The mixture was first ball-milled for 24h with yttria-stabilized zirconia balls using ethanol as the milling medium. After removing the ethanol via a drying step at 100 °C, the powder was lightly ground then calcined at 1100 °C for 10h (5°C/min for heating and cooling rates). The milling and calcination steps were repeated a second time to ensure phase formation. A green compact was prepared from the resulting powder by first applying uniaxial pressure of 20 MPa in a cylindrical die, then applying ~ 250 MPa in an isostatic press. The green body was sintered at 1600 °C for 12 ~ 24 h, during which the sample was entirely covered with a mixture of powder of the same composition and excess barium carbonate to avoid barium loss to evaporation<sup>42</sup>. The covering powder was firmly compacted by lightly pressing the die shaft onto the powder inside the sintering crucible.

The conductivity of the BZCY442, BZCYb442, BZCHo442, and BZCYYb4411 samples was measured by impedance spectroscopy over the frequency range of 5 MHz to 10 Hz using a Biologic (SP-300) with an applied alternating current (ac)

voltage amplitude of 20 mV. Silver paint (SPI, Product 05063-AB) electrodes were applied onto both surfaces of the polished sample. The impedance spectra were collected under a water-saturated  $\rm N_2$  atmosphere ( $p\rm H_2O=0.031$  atm) from 100 to 600 °C. For the chemical stability under CO $_2$ , mass changes in BZCYYb4411 and BZCYYb1711 were measured by thermogravimetric analysis (TGA) using a Netzsch STA (simultaneous thermal analyzer) 449 C and powder samples. The temperature was increased from 100 to 500 °C with 2 °C min^-1 in  $\rm N_2$  and held for 8 hours in 60 % CO $_2$  balanced in  $\rm N_2$ . Subsequent to the TGA experiment, the XRD pattern of the BZCYYb1711 sample was collected. Further, the XRD patterns of BZCY442, BZCH0442, BZCHVb441, BZCYYb4411 samples were measured before and after exposure to 100% CO $_2$  at 500 °C.

Conventional fuel cell fabrication. Anode-supported full cells with a configuration of NiO-BZCYYb4411/BZCYYb4411/PBSCF and NiO-BZCYYb1711/BZCYYb1711/PBSCF were fabricated using a drop-coating method to conduct fuel cell measurements. The anode was formed from in-house synthesized NiO and electrolyte powders (BZCYYb4411 and BZCYYb1711), the former by the glycine nitrate process, and the latter by typical solid state reaction method. For NiO synthesis, nickel nitrate was dissolved in distilled water and glycine was added in the solution in a 1:1 molar ratio. The solution was heated on a hot plate set at 350 °C to evaporate water, yielding a viscous liquid. Fine NiO powders were obtained via a subsequent combustion reaction. The resulting NiO powder was calcined at 800 °C for 4h in air. The NiO-BZCYYb4411 and NiO-BZCYYb1711 composite anodes were prepared by ball milling NiO powder, electrolyte powders (BZCYYb4411 and BZCYYb1711), and starch in a weight ratio of 65:35:0.5 in ethanol for 24 h. After a drying step, the composite powders were mechanically pressed into a disc and lightly sintered at 800 °C for 4 h.

A thin electrolyte layer (either BZCYYb4411 or BZCYYb1711) was applied atop the porous anode by a drop coating technique. Specifically, the electrolyte powder was suspended in a multi-component organic fluid in a 1:10 solid-to-fluid weight ratio, where the fluid was comprised of a mixture of 2-butanol binder (Alfa Aesar), polyvinyl butyral (Tape Casting Warehouse, TCW), butyl benzyl phthalate (TCW), polyalkylene glycol (TCW), and triethanolamine (Alfa Aesar). After drop-coating onto the lightly fired anode support, the resulting anode/ electrolyte bi-layer was heat-treated at 400 °C for 1 h to remove organics. Sintering was carried out immediately thereafter in a two-step protocol in which the sample was first exposed to 1550 °C for 2 min and then 1500 °C (BZCYYb4411) and 1400 °C (BZCYYb1711) for 4h to maximize grain growth while minimizing barium volatilization. The resulting electrolyte thickness was ~15 μm. The cathode layer was applied in the form of a slurry, comprised of a mixture of PBSCF powder and the organic binder, V-006 (Heraeus) in a 1:1.2 ratio. After slurry deposition onto the electrolyte layer, the complete cell was sintered at 950 °C for 4 h in air, resulting in a cathode layer ~20 µm thick with an effective area of 0.28 cm2. The microstructures and morphologies were observed using a field emission scanning electron microscope (SEM) (Hitachi SU8030).

Fuel cell fabrication with pulsed laser deposition (PLD) layer. To facilitate PLD of PBSCF, large targets of the material were fabricated. Pre-calcined PBSCF powders were mechanically pressed into discs by uniaxial press (20 MPa for 1 min) then further pressed in an isostatic press (~250 MPa for 20 min). Green bodies were sintered at 1150 °C for 12 h to yield compacts ~ 24 mm in diameter and 4-5 mm in thickness. Typical densities were ~95 % of theoretical, as determined by the Archimedes method. PBSCF films were grown on the electrolyte side of NiO+BZCYYb4411/BZCYYb4411 bi-layer cells using a PVD PLD/MBE 2300 in the Northwestern University PLD core facility. The substrate was heated at a rate of 30 °C/min temperature and the temperature fixed at 650 °C for growth. The oxygen pressure in the chamber was set at 30 mTorr. The growth rate was found to be 20.8 nm min<sup>-1</sup> for the conditions employed (248 nm KrF laser, 270 mJ/ pulse, 10 Hz repetition rate). Upon completion of the deposition, the chamber was vented to 300 Torr oxygen pressure, to facilitate oxidation of the film, and cooled at a rate of 10 °C/min. As with the conventional cells, a slurry of PBSCF was then brush-painted (now onto the PBSCF thin film rather than the electrolyte) and the complete cell was sintered at 950 °C for 4 hours in air.

**Fuel cell electrochemical characterization.** Ag wires (GoodFellow) were attached at both electrodes of single cell using an Ag paste (SPI supplies) as a current collector. An alumina tube and a ceramic adhesive (Ceramabond 552, Aremco) were employed to fix and seal the single cell. Humidified hydrogen (3% H<sub>2</sub>O) was applied as fuel to the anode through a water bubbler with a flow rate of 60 sccm and air was supplied to cathode with a flow rate of 200 sccm during single cell tests. Impedance spectra were recorded under open circuit voltage (OCV) in a frequency range of 100 kHz to 0.1 Hz with AC perturbation of 20 mV. *I-V* curves were collected using a BioLogic SP-300 Potentiostat at operating temperature from 500 to 650 °C in intervals of 50 °C. The current stability was measured under a fixed voltage of 0.5 V at 550 °C. The open circuit stability was measured for BZCYYb4411 and BZCYYb1711 electrolyte-based fuel cells with humidified (3% H<sub>2</sub>O) 10 % CO<sub>2</sub> and 90 % H<sub>2</sub> mixture at 500 °C supplied to the anode and air to the cathode.

Microelectrode preparation and characterization. Electrochemical characterization was performed on an array of PBSCF microdots supported on a proton-conducting electrolyte substrate. Initial experiments in this work began with the electrolyte BZCYYb1711 and thus this material served as the substrate. A dense compact of BZCYYb1711 ~1.5 mm in thickness was prepared by the methods described above (solid state synthesis, final sintering at 1600 °C for 18h). To provide a smooth surface for electrode deposition, a thin (~250 nm) buffer layer of BaZr<sub>0.8</sub>Y<sub>0.2</sub>O<sub>3</sub> was applied by a custom-made PLD/Laser-MBE System (Pascal Co., Ltd.) equipped with a loadlock chamber using a target prepared by chemical solution method which is described in detail elsewhere (16). A KrF (λ=248 nm) excimer laser (Lambda COMPexPro) was used to ablate the targets at a pulse repetition rate of  $5\,\mathrm{Hz}$ , a laser fluence of  $0.51\,\mathrm{J/cm^2}$  and a target-substrate distance ~55 mm. Following the deposition of buffer layer, a thin film (~600 nm) of PBSCF was deposited on top using a target identical to the type used for PLD-modification of fuel cells. The growth rate of BZY and PBSCF was determined to be  $2\,\mathrm{nm}\;\mathrm{min^{-1}}$  and  $2.6\,\mathrm{nm}\;\mathrm{min^{-1}}$ , respectively, for the following growth conditions: oxygen pressure: 30 mTorr for BZY, 100 mTorr for PBSCF; laser fluence on target: 0.51 J cm<sup>-2</sup>; laser power: 25 mJ; repeat rate: 5 Hz; substrate temperature: ~680 °C for BZY, ~640 °C for PBSCF. The grown film was then characterized by XRD (Bruker D8 Discover with 4 bounce monochromator, Cu Kα radiation), optical microscopy (Keyence VW-9000), and atomic force microscopy (AFM, Digital Instruments Nanoscope III and Dimension 5000). For electrochemical characterization the film was patterned, using photolithography and ion milling, into a library of microelectrodes with diameters spanning from 125 to 500 μm. Specifically, each sample was coated with a photoresist (Shipley 1813) by a regular spin coating method (4000 rpm for 50 s). After spin coating, the photoresist was baked at 100 °C for 2 min to drive off solvents and to solidify the film, following an exposure to UV radiation for 12 s through a photomask, and then developed in Shipley 352 developer for 40 s. The sample then underwent ion milling for 90 min, resulting in a milling depth of 650 nm. In the final step, the residual photoresist was stripped using acetone. After the patterning, a circular microelectrode array with diameters of  $125\text{--}500\,\mu m$ was well defined on the top of BZCYYb1711. Impedance data were collected at a film temperature of 500 °C ( $pO_2 = 0.2$  atm and  $pH_2O = 0.016$  atm) over the frequency range 1 MHz to 32 mHz using a voltage amplitude of 30 mV under zero-bias conditions (Solartron 1260). The data acquisition in an automated impedance microprobe instrument is described in detail elsewhere<sup>39</sup>.

**Data availability.** The data that support the plots within this paper and other findings of this study are available from the corresponding author upon reasonable request.

Received: 18 August 2017; Accepted: 18 December 2017; Published online: 12 February 2018

#### References

- Fabbri, E., Pergolesi, D. & Traversa, E. Materials challenges toward proton-conducting oxide fuel cells: a critical review. *Chem. Soc. Rev.* 39, 4355–4369 (2010).
- 2. Nguyen, N. T. Q. & Yoon, H. H. Preparation and evaluation of  $BaZr_{0.1}Ce_{0.7}Y_{0.1}Yb_{0.1}O_{1.5}$  (BZCYYb) electrolyte and BZCYYb-based solid oxide fuel cells. *J. Power Sources* **231**, 213–218 (2013).
- Duan, C. et al. Readily processed protonic ceramic fuel cells with high performance at low temperatures. *Science* 349, 1321–1326 (2015).
   Nien, S. H., Hsu, C. S., Chang, C. L. & Hwang, B. H. Preparation of
- Nien, S. H., Hsu, C. S., Chang, C. L. & Hwang, B. H. Preparation of BaZr<sub>0.1</sub>Ce<sub>0.7</sub>Y<sub>0.2</sub>O<sub>3.5</sub> based solid oxide fuel cells with anode functional layers by tape casting. *Fuel Cells* 11, 178–183 (2011).
- Bae, K. et al. Demonstrating the potential of yttrium-doped barium zirconate electrolyte for high-performance fuel cells. *Nat. Commun.* 8, 14553 (2017).
- 6. Yoo, S., Choi, S., Kim, J., Shin, J. & Kim, G. Investigation of layered perovskite type  $NdBa_{1-x}Sr_xCo_2O_{5+\delta}$  (x=0,0.25,0.5,0.75, and 1.0) cathodes for intermediate-temperature solid oxide fuel cells. *Electrochim. Acta* **100**, 44–50 (2013).
- Liu, Q. L., Khor, K. A. & Chan, S. H. High-performance low-temperature solid oxide fuel cell with novel BSCF cathode. *J. Power Sources* 161, 123–128 (2006).
- Shao, Z. & Haile, S. M. A high-performance cathode for the next generation of solid-oxide fuel cells. *Nature* 431, 170–173 (2004).
- 9. Choi, S. et al. Highly efficient and robust cathode materials for low-temperature solid oxide fuel cells:  $PrBa_{0.5}Sr_{0.5}Co_{2-x}Fe_xO_{5+\delta}$ . Sci. Rep. 3, 2426 (2013).
- Fabbri, E., Markus, I., Bi, L., Pergolesi, D. & Traversa, E. Tailoring mixed proton-electronic conductivity of BaZrO<sub>3</sub> by Y and Pr co-doping for cathode application in protonic SOFCs. Solid State Ion. 202, 30–35 (2011).
- 11. Wang, Z. et al. A mixed-conducting  $BaPr_{0.8}In_{0.2}O_{3-\delta}$  cathode for proton-conducting solid oxide fuel cells. *Electrochem. Commun.* 27, 19–21 (2013).

Han, D., Okumura, Y., Nose, Y. & Uda, T. Synthesis of La<sub>1-x</sub>Sr<sub>x</sub>Sc<sub>1-y</sub>Fe<sub>y</sub>O<sub>3-5</sub> (LSSF) and measurement of water content in LSSF, LSCF and LSC hydrated in wet artificial air at 300°C. Solid State Ion. 181, 1601–1606 (2010).

- Grimaud, A. et al. Hydration and transport properties of the Pr<sub>2-x</sub>Sr<sub>x</sub>NiO<sub>4+δ</sub> compounds as H+-SOFC cathodes. *J. Mater. Chem.* 22, 16017–16025 (2012).
- Grimaud, A. et al. Hydration properties and rate determining steps of the oxygen reduction reaction of perovskite-related oxides as H+-SOFC cathodes. J. Electrochem. Soc. 159, B683–B694 (2012).
- Strandbakke, R. et al. Gd- and Pr-based double perovskite cobaltites as oxygen electrodes for proton ceramic fuel cells and electrolyser cells. Solid State Ion. 278, 120–132 (2015).
- Fabbri, E., D'Epifanio, A., Di Bartolomeo, E., Licoccia, S. & Traversa, E.
   Tailoring the chemical stability of Ba(Ce<sub>0.8-x</sub>Zr<sub>x</sub>)Y<sub>0.2</sub>O<sub>3-5</sub> protonic conductors for Intermediate Temperature Solid Oxide Fuel Cells (IT-SOFCs). Solid State Ion. 179, 558–564 (2008).
- Yang, L. et al. Enhanced sulfur and coking tolerance of a mixed ion conductor for SOFCs: BaZr<sub>0.1</sub>Ce<sub>0.7</sub>Y<sub>0.2-x</sub>Yb<sub>x</sub>O<sub>3-δ</sub>. Science 326, 126–129 (2009).
- Haile, S. M., Staneff, G. & Ryu, K. H. Non-stoichiometry, grain boundary transport and chemical stability of proton conducting perovskites. *J. Mater.* Sci. 36, 1149–1160 (2001).
- Takayama-Muromachi, E. & Navrotsky, A. Energetics of compounds (A<sup>2+</sup>B<sup>4+</sup>O<sub>3</sub>) with the perovskite structure. *J. Solid State Chem.* 72, 244–256 (1988).
- Ryu, K. H. & Haile, S. M. Chemical stability and proton conductivity of doped BaCeO<sub>3</sub>-BaZrO<sub>3</sub> solid solutions. Solid State Ion. 125, 355–367 (1999).
- Yamazaki, Y., Hernandez-Sanchez, R. & Haile, S. M. High total proton conductivity in large-grained yttrium-doped barium zirconate. *Chem. Mater.* 21, 2755–2762 (2009).
- Bozza, F., Arroyo, Y. & Graule, T. Flame spray synthesis of BaZr<sub>0.8</sub>Y<sub>0.2</sub>O<sub>3.6</sub> electrolyte nanopowders for intermediate temperature proton conducting fuel cells. Fuel Cells 15, 588–594 (2015).
- 23. Ling, Y., Yu, J., Zhang, X., Zhao, L. & Liu, X. A cobalt-free  $\rm Sm_{0.5}Sr_{0.5}Fe_{0.8}Cu_{0.2}O_{3-6}-Ce_{0.8}Sm_{0.2}O_{2-6}$  composite cathode for proton-conducting solid oxide fuel cells. *J. Power Sources* **196**, 2631–2634 (2011).
- Kim, J. et al. Triple-conducting layered perovskites as cathode materials for proton-conducting solid oxide fuel cells. *ChemSusChem* 7, 2811–2815 (2014).
- 25. Choi, S., Shin, J. & Kim, G. The electrochemical and thermodynamic characterization of PrBaCo<sub>2-x</sub> Fe<sub>x</sub>O<sub>5+δ</sub> (x= 0, 0.5, 1) infiltrated into yttria-stabilized zirconia scaffold as cathodes for solid oxide fuel cells. *J. Power Sources* 201, 10–17 (2012).
- 26. Kim, G. et al. Rapid oxygen ion diffusion and surface exchange kinetics in PrBaCo<sub>2</sub>O<sub>5+x</sub> with a perovskite related structure and ordered A cations. J. Mater. Chem. 17, 2500–2505 (2007).
- Kim, J. H., Cassidy, M., Irvine, J. T. & Bae, J. Electrochemical investigation of composite cathodes with SmBa<sub>0.5</sub>Sr<sub>0.5</sub>Co<sub>2</sub>O<sub>5+6</sub> cathodes for intermediate temperature-operating solid oxide fuel cell. *Chem. Mater.* 22, 883–892 (2009).
- Jun, A. et al. Correlation between fast oxygen kinetics and enhanced performance in Fe doped layered perovskite cathodes for solid oxide fuel cells. J. Mater. Chem. A 3, 15082–15090 (2015).
- Kim, J.-H. & Manthiram, A. Layered LnBaCo<sub>2</sub>O<sub>5+6</sub> perovskite cathodes for solid oxide fuel cells: an overview and perspective. *J. Mater. Chem. A* 3, 24195–24210 (2015).
- 30. Jeong, D. et al. Structural, electrical, and electrochemical characteristics of  $LnBa_{0.5}Sr_{0.5}Co_{1.5}Fe_{0.5}O_{5.46}$  (Ln=Pr, Sm, Gd) as cathode materials in intermediate-temperature solid oxide fuel cells. *Energy Technol.* 5, 1337–1343 (2017).
- Kim, J.-H., Prado, F. & Manthiram, A. Characterization of GdBa<sub>1-x</sub>Sr<sub>x</sub>Co<sub>2</sub>O<sub>5+δ</sub> (0≤x≤1.0) double perovskites as cathodes for solid oxide fuel cells. *J. Electrochem. Soc.* 155, B1023–B1028 (2008).
- Burriel, Mn et al. Anisotropic oxygen ion diffusion in layered PrBaCo<sub>2</sub>O<sub>5+δ</sub>. Chem. Mater. 24, 613–621 (2012).
- Hashimoto, D., Han, D. & Uda, T. Dependence of lattice constant of Ba, Co-contained perovskite oxides on atmosphere, and measurements of water content. Solid State Ion. 262, 687–690 (2014).
- Yamazaki, Y., Babilo, P. & Haile, S. M. Defect chemistry of yttrium-doped barium zirconate: a thermodynamic analysis of water uptake. *Chem. Mater.* 20, 6352–6357 (2008).
- Yamazaki, Y., Yang, C.-K. & Haile, S. M. Unraveling the defect chemistry and proton uptake of yttrium-doped barium zirconate. Scr. Mater. 65, 102–107 (2011).
- Poetzsch, D., Merkle, R. & Maier, J. Proton uptake in the H<sup>+</sup>-SOFC cathode material Ba<sub>0.5</sub>Sr<sub>0.5</sub>Fe<sub>0.8</sub> Zn<sub>0.2</sub>O<sub>3-5</sub>: transition from hydration to hydrogenation with increasing oxygen partial pressure. *Faraday Discuss.* 182, 129–143 (2015).

- 37. Zohourian, R., Merkle, R. & Maier, J. Proton uptake into the protonic cathode material  $BaCo_{0,4}Fe_{0,4}$   $Zr_{0,2}O_{3.5}$  and comparison to protonic electrolyte materials. *Solid State Ion.* **299**, 64–69 (2017).
- Hildenbrand, N., Boukamp, B. A., Nammensma, P. & Blank, D. H. Improved cathode/electrolyte interface of SOFC. Solid State Ion. 192, 12–15 (2011).
- 39. Usiskin, R. E., Maruyama, S., Kucharczyk, C. J., Takeuchi, I. & Haile, S. M. Probing the reaction pathway in  $(La_{0.8}Sr_{0.2})_{0.95}MnO_{3+6}$  using libraries of thin film microelectrodes. *J. Mater. Chem. A* **3**, 19330–19345 (2015).
- 40. Newman, J. Resistance for flow of current to a disk. J. Electrochem. Soc. 113, 501–502 (1966).
- Pechini, M. P. Method of preparing lead and alkaline earth titanates and niobates and coating method using the same form a capacitor. US Patent 3.330.697 (1967).
- 42. Babilo, P., Uda, T. & Haile, S. M. Processing of yttrium-doped barium zirconate for high proton conductivity. *J. Mater. Res.* 22, 1322–1330 (2007).

# Acknowledgements

This research was funded in part by the US Department of Energy, through ARPA-e Contract DE-AR0000498, via subcontract from United Technologies Research Center, and

by the National Science Foundation, DMR-1505103. Selected facilities used were supported by the National Science Foundation via Northwestern University's MRSEC, DMR-1121262.

#### Author contributions

S.M.H led the development of the concept, guided the experimental design, and supervised the research. S.C. developed the materials, fabricated the cells, and performed the following experiments and analyses: conductivity, thermogravimetry, fuel cell polarization, and impedance spectroscopy. Y.L. and X.Z. prepared and characterized PLD microdot electrodes, on which C.J.K. performed electrochemical measurements. I.T. supervised PLD film growth and characterization. H.-I. J. provided critical suggestions for experimental and analytical methods. S.M.H. and S.C. wrote the paper with contributions from all authors.

## Additional information

**Supplementary information** is available for this paper at https://doi.org/10.1038/ $\pm$ 41560-017-0085-9.

Reprints and permissions information is available at www.nature.com/reprints.

Correspondence and requests for materials should be addressed to S.M.H.

**Publisher's note:** Springer Nature remains neutral with regard to jurisdictional claims in published maps and institutional affiliations.